Photovoltaic performance of CdS/CdTe junctions on ZnO nanorod arrays

G. Kartopu[a,*], D. Turkay[b,c], C. Ozcan[b,d], W. Hadibrata[b,c], P. Aurang[b,c], S. Yerci[b,c,d], H.E. Unalan[b,c,e], V. Barrioz[f], Y. Qu[f], L. Bowen[g], A.K. Gürlek[a], P. Maiello[f], R. Turan[b,c,h], S.J.C. Irvine[a]

[a] Centre for Solar Energy Research, College of Engineering, Swansea University, OpTIC Centre, St. Asaph Business Park, LL17 0JD, UK
[b] Centre for Solar Energy Research and Applications (GÜNAM), Middle East Technical University, 06800 Ankara, Turkey
[c] Department of Micro and Nanotechnology, Middle East Technical University, 06800 Ankara, Turkey
[d] Department of Electrical and Electronics Engineering, Middle East Technical University, 06800 Ankara, Turkey
[e] Department of Metallurgical and Materials Engineering, Middle East Technical University, 06800 Ankara, Turkey
[f] Department of Mathematics, Physics and Electrical Engineering, Ellison Building, Northumbria University, Newcastle Upon Tyne NE1 8ST, UK
[g] G.J. Russell Microscopy Facility, Durham University, South Road, Durham DH1 3LE, UK
[h] Department of Physics, Middle East Technical University, 06800 Ankara, Turkey

ARTICLE INFO

ABSTRACT

One-dimensional nanostructures, such as nanorod (NR) arrays, are expected to improve the photovoltaic (PV) response of solar cells with an ultrathin absorber due to an increased areal (junction) density and light trapping. We report on the deposition of CdS and CdTe:As semiconductor thin films on ZnO NR arrays by means of metalorganic chemical vapour deposition (MOCVD). The change in optical properties of the ZnO NRs upon the growth of CdS shell was monitored and compared to the simulated data, which confirmed the presence of strong light scattering effects in the visible and near infrared regions. The PV performance of nanostructured *vs.* planar CdS/CdTe solar cells (grown using the material from the same MOCVD run) showed similar conversion efficiencies (~ 4%), despite the current density being lower for the nanostructured cell due to its thicker CdS window. A clear improvement in the quantum efficiency was however observed in the near infrared region, resulting from the light trapping by the ZnO/CdS core-shell NR structure. We also showed that reduction of surface defects and use of high absorber carrier density would boost the efficiency beyond that of planar CdTe solar cells. The reported device performance and the direct observation of light trapping are promising towards optimisation of extremely-thin-absorber CdTe PV devices.

1. Introduction

Cadmium telluride (CdTe) based photovoltaic technology is increasing its promise for large scale solar electricity production, with new record efficiencies of 22.1% for solar cells and 18.6% for modules [1]. Although, only 1 µm thick CdTe is sufficient to capture more than 95% of the solar spectrum above the CdTe bandgap (1.45 eV), typically more than 2 µm thick CdTe is used to realise high efficiency planar devices. Attempts to reduce the CdTe thickness to less than 1 µm so far ended with severe losses in cell performance [2].

Electrically conducting ZnO nanorod (NR) arrays would form an interesting front contact for superstrate CdTe solar cells with an extremely-thin-absorber (eta). A combination of the improved areal density of the semiconductor junction (due to the large surface area of the NR array available for deposition) and also the light trapping effects observable in such nanostructures [3] are expected to improve the

photocurrent and spectral response. However, a survey of the related literature on solar cells involving NR arrays (Table 1) suggests this is not straightforward to realise. In practice, there seems to be many technical issues related to material properties and deposition uniformity, resulting in poor and even non-functional one-dimensional PV structures. The best result was obtained by depositing a thick CdTe layer, via chemical vapour deposition, onto CdS nanopillars sticking out of a porous anodic alumina nano-template [9]. However, this process is very complicated involving many fabrication steps. Simplified structures to be deposited by highly conformal deposition methods, such as atomic layer deposition (ALD), metalorganic chemical vapour deposition (MOCVD), and successive ionic layer adsorption and reaction (SILAR), would be of interest to advance one-dimensional CdTe photovoltaics.

This paper presents a study into the effects of using a ZnO NR scaffold on the growth and performance of CdS/CdTe solar cells,

Table 1
Comparative performance of CdTe based one-dimensional photovoltaics.

Substrate	Structure	Absorber		J_{sc} (mA cm^{-2})	η (%)	Ref
		Growth method	Thickness (μm)			
Various	Dense CdTe NR	MS	0.1	0.04	–	[4]
FTO/glass	ZnO/CdTe NR	CSS	0.05–0.1	0.35	0.01	[5]
ITO/glass	ZnO/CdTe NR	ED	~0.1	5.9	–	[6]
FTO/glass	ZnO/CdS/CdTe NR	SILAR	~0.2	~8	0.7	[7]
Mo/glass	CdTe/CdS/ZnO/ITO NR	VLS (via CSS)	0.05–0.2	13.9	2.49	[8]
AAO/Al	CdS/CdTe NR	CVD	1	21	6	[9]

TF, Thin Film; NR, Nanorod; ITO, Indium Tin Oxide; FTO, Fluorine-doped Tin Oxide; Mo, Molybdenum; AAO, Anodic Aluminium Oxide; Al, Aluminium; MS, Magnetron Sputtering; ED, Electro-chemical Deposition; CSS, Closed-Space Sublimation; VLS, Vapour-liquid-solid growth; CVD, Chemical Vapour Deposition.

deposited by MOCVD. A ZnO/CdS/CdTe core-shell NR based device structure, modelled using the finite-difference time-domain (FDTD) method for light-trapping prediction, was fabricated using hydrothermal and MOCVD methods for the deposition of ZnO and CdS/CdTe, respectively. The deposition characteristics of the CdS/CdTe shells on the ZnO NRs, as well as their material properties were assessed. Nanostructured solar cells, with comparable performance to planar cells and displaying light trapping characteristics are reported. Thin film properties and device performance issues are discussed for the future optimisation of eta-CdTe cells.

2. Experimental and simulation details

ZnO NRs aligned perpendicularly to the substrate were synthesized via a hydrothermal method [10]. First, a ~ 10 nm thick ZnO film, serving as the self-catalytic seed layer for the ZnO NR growth, was deposited by radio-frequency magnetron sputtering (6 sccm Ar flow, 40 W power, 25 mTorr pressure) onto a commercial indium tin oxide (ITO)/boro-aluminosilicate glass (Delta Technologies, 4–8 Ω/sq. with 83% transparency at 550 nm). The seed layer coated substrate was then dipped into the hydrothermal solution containing 19 mM zinc acetate dihydrate [Zn(O$_2$CCH$_3$)$_2$(H$_2$O)$_2$], 1 mM aluminium acetate [Al (C$_2$H$_3$O$_2$)$_3$] and 20 mM hexamethylene tetramine (C$_6$H$_{12}$N$_4$), and kept at 80 °C for 45–180 min. The substrates taken from the solution were washed in de-ionised water and dried under N$_2$ gas. The growth duration determines the length of NRs, where the amount of hexamethylene tetramine determines the rod diameter. Using this method one can easily grow ZnO NR array films over relatively large areas (few cm^2) with high uniformity (in rod height and diameter), as depicted in Ref. [10]. In this study, the NR length was controlled in the range of 0.5–1.4 μm.

A conventional (horizontal, atmospheric pressure) MOCVD reactor was used to deposit CdS/CdTe layers as well as to perform CdCl$_2$ activation treatment for the devices. The CdS film was deposited without pre-treatment on the ZnO NRs using ditertiarybutylsulphide and dimethylcadmium organometallic precursors and hydrogen (H$_2$) carrier gas at 315 °C. CdTe films were deposited at 390 °C with ~ 10^{19} atoms cm^{-3} arsenic (As) dopant atoms incorporated. The precursors for As and Te were tris(dimethylamino)arsenic and diisopropyltelluride, respectively. Device activation was performed in two steps; first, a CdCl$_2$ layer was deposited onto the CdTe surface at 200 °C, using tertiarybutylchloride as the Cl source, and annealed for 3 min at 420 °C (in H$_2$ atmosphere), and second, the sample was annealed in air at 170 °C for 90 min after being taken out of the MOCVD chamber. Further experimental details on MOCVD growth and device activation can be found in Refs. [11,12].

Solar cells were defined by evaporating Au through a shadow mask onto the air-annealed CdTe surfaces. The cells were typically dot contact type with a diameter of 2 mm (3.14 mm^2 area), but larger ones with 5 mm × 5 mm (25 mm^2 area) dimensions were also used for spectral response measurements. AM1.5G *J-V* curves were collected

using an Abet Technologies Ltd. solar simulator with the light power density calibrated using a GaAs reference cell. External quantum efficiency (*EQE*) measurements were carried out using a Bentham spectral response system under unbiased conditions over the spectral range 300–1000 nm. The system response was corrected by scanning the output of a c-Si reference detector. Arsenic atom concentration depth profiling was carried out via secondary ion-mass spectroscopy (SIMS) using a Cameca IMS-4f instrument with Cs$^+$ ion source operating with 10 keV energy and 20 nA current. UV–Vis spectroscopy (Shimadzu UV-2600, Varian Cary5000) was used to measure both transmittance and haze of the ZnO NRs before and after CdS deposition. Electrical properties of the ZnO NRs/ITO substrates were characterised by four point probe (for sheet resistance) and the Hall effect (for carrier density and mobility) measurements at room temperature. Prior to electrical measurements, the samples were spin coated with a dilute poly(methyl methacrylate) (PMMA) solution in chlorobenzene at 3000 rev min^{-1} and allowed to dry in air, in order to partly fill the gaps between NRs for complete electrical isolation of the underlying ITO film. Scanning electron microscopy (Tescan Mira 3, Zeiss EVO HD 15, FEI Helios NanoLab) and transmission electron microscopy (JEOL JEM 2100F) were used in combination with high resolution/low voltage energy-dispersive X-ray spectroscopy (EDS, Oxford Instruments X-Max Extreme) to characterise the structure and composition of the samples. For TEM analysis, samples were scraped off the ITO substrates, sonicated in isopropanol and drop casted onto copper grids.

The optical simulations of the structures were performed using a commercially available finite-difference time-domain (FDTD) simulation tool, LUMERICAL™. A full-field electromagnetic wave calculation was carried out. The size of the unit cell was set to be 2000 nm × 2000 nm. Plane waves were normally directed into the structure in the z-direction (i.e. from the glass side). Bloch periodic boundary conditions were set in x- and y-direction. Meanwhile, perfectly matched layers (PMLs) were utilized in the direction of propagation of the plane waves. The haze simulations of ZnO rods and CdS/ZnO rods were carried out in three-dimensional layouts with cubic mesh size of 5 nm. This structure consists of randomized rods, whose coordinates were generated using a randomization algorithm with minimum separation between each rod specified at 100 nm.

In optical simulations of CdTe solar cells, the geometrical parameters of the cell structure were extracted from the cross-sectional EDS images. The ZnO NR diameters were measured as 100 nm with an average height of 470 nm and the average deviation of the NRs from the surface normal was measured as ~ 20°. The average CdTe layer thickness was found to be 830 nm. The conformal CdS window layer of 20 nm thickness was built around the ZnO NRs. The CdTe layer is thick enough to 'bury' all the ZnO/CdS NRs, yielding an excess layer of 360 nm. Optical simulations for planar solar cells were performed for comparison. For the planar cells, ZnO and CdS thicknesses were kept as 10 nm and 20 nm, respectively, as in the NR-based cells. The CdTe thickness was chosen by considering the equivalent volume of CdTe used in the NR-based cells. The corresponding planar CdTe thickness

was calculated as 530 nm. The calculation of absorption for CdTe/CdS/ZnO solar cells was performed on a 2D structure with square mesh of 1 nm. ITO, ZnO, CdS, CdTe and Au material properties were taken from Refs. [13–16].

The electrical simulations were carried out using Silvaco ATLAS. A periodic structure was assumed to reduce the computational cost. We expect that the randomness should not affect the electrical simulation results as long as the total surface area is kept constant. The period was chosen as the average distance between nanorods in the random structure. Photo-generated current densities in each layer for random structures were extracted by optical simulations. Optical generation profiles for periodic structures were provided to the electrical simulations as an input, and the generation rates were scaled in each layer to match the photo-generated current densities in the random structures. Bandgap, electron affinity, relative dielectric permittivity, conduction and valence band density of states, electron and hole mobility values, and defect parameters for CdTe, CdS, ZnO and ITO, Au were extracted from the literature (Ref. [17–21]) and provided in Tables S1-3 (Supplementary file).

3. Results and discussion

The following sections describe the structural, optical and electrical properties of the prepared one-dimensional materials as well as the solar cell device performance using an eta CdTe film.

3.1. ZnO NR arrays

From SEM images, such as those shown in Fig. 1, the near-perpendicular orientation of the NRs on the growth substrate was confirmed. However, in view of the subsequent deposition of CdS shells, it is important to note that the gap between the rods actually varied from several nanometers up to 0.3 μm, due to the varying misalignment of the NRs in the out-of-plane direction. The mean rod diameter for a NR length of 0.75 μm (Fig. 1c) was determined to be ~ 50 nm.

After the growth of ZnO NRs on the ITO/glass substrate, the sheet resistance was observed to increase from ~8 to 20 Ω/□, while the carrier density decreased from 1.2×10^{21} to 1.3×10^{20} cm^{-3} and the electron mobility increased from 41 to 44 cm^2 V^{-1} s^{-1}.

3.2. ZnO/CdS core-shell NRs

In general, very rapid nucleation and high growth rates were observed for CdS deposition onto ZnO NRs, in comparison to planar reference substrates (Fig. 2a). This is consistent with the behaviour expected for surface kinetic limited growth. In some cases, this resulted in complete filling of the gaps between the ZnO NRs (Fig. 2b, c), even though only 50 nm film was grown on the planar reference. Reduction of the deposition time, i.e. thickness on the reference substrate (Fig. 2d), allowed formation of CdS/ZnO core-shell NRs: presence of large gaps between the ZnO NRs (Fig. 2e) and formation of a distinct, uniform shell around single NRs (Fig. 2f) following CdS deposition were observable. However, the substrate coverage became uneven (Fig. 2d), which resulted in the variation of shell thickness.

The EDS spectra confirmed the shell composition to be stoichiometric CdS, as shown in Fig. 3a. The ZnO core region in HRTEM image (Fig. 3b) showing (002) planes (0.266 ± 0.77 nm separation) being parallel to the NR growth direction. The CdS shell (~ 5 nm) was observed to have high degree of crystallinity, with its (113) plane (0.189 ± 0.73 nm separation) aligned with the (002) ZnO planes (both materials are assumed to have the usual hexagonal wurtzite structure).

The transition in the total (direct and scattered) and scattered light transmittance of the ITO/glass substrate upon the sequential deposition ZnO NRs and ZnO/CdS core-shell NRs are shown in Fig. 4, together with optical simulations. In general, a good agreement between experimental and simulated results are obtained. Compared to pristine ITO/glass substrate (not shown), the growth of ZnO NRs shifted the high energy absorption edge towards the ZnO band edge (~ 370 nm) and induced significant haze in the visible range (Fig. 4a), giving the samples a milky appearance. For the 0.5 μm length ZnO NRs, the total transmittance remained as high as that of starting substrate. If the NR length is increased to 1.4 μm, the total transmittance reduced at most wavelengths, with a maximum of $T \approx 80\%$ at 900–1100 nm, and the intensity of the scattered light increased significantly. The absorption onset shifted to the CdS bandgap (~ 520 nm), transmittance reduced further ($T_{max} \approx 65\%$ at 700–870 nm), and both the intensity and width of the scattering component increased on the growth of CdS shells on ZnO NRs (Fig. 4b). The strong scattering observed is a desirable effect for a thin solar absorber to be deposited onto the ZnO/CdS core-shell NRs array in order to increase the absorption in the CdTe film.

3.3. CdTe absorber deposition

CdTe:As films were grown on ZnO NRs for the assessment of their deposition behaviour and material properties. The SIMS depth profiling (Fig. 5a) shows that the elements due to ZnO and CdTe:As materials co-exist from the back surface down to the ITO/glass interface, confirming the conformal deposition of CdTe onto ZnO NRs with MOCVD (Fig. 5b).
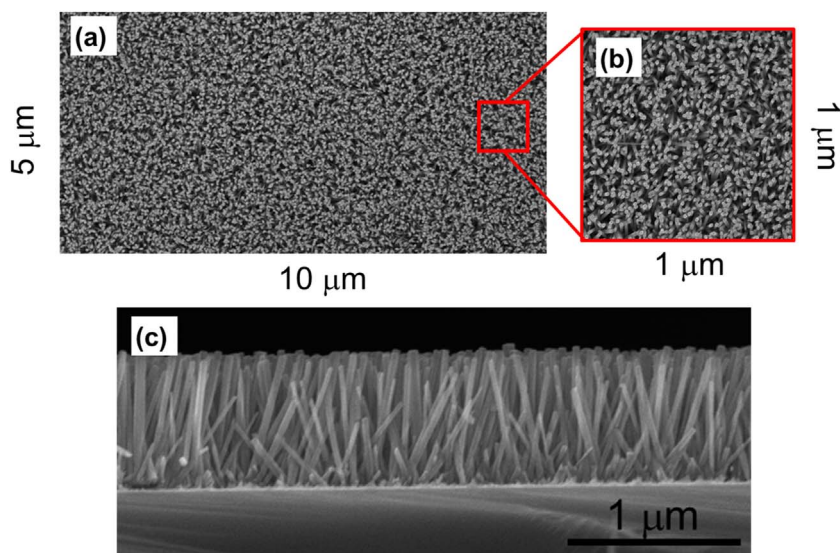

Fig. 1. Top view (a, b) and cross-sectional SEM images (c) of the ZnO NRs with 0.8 μm length.
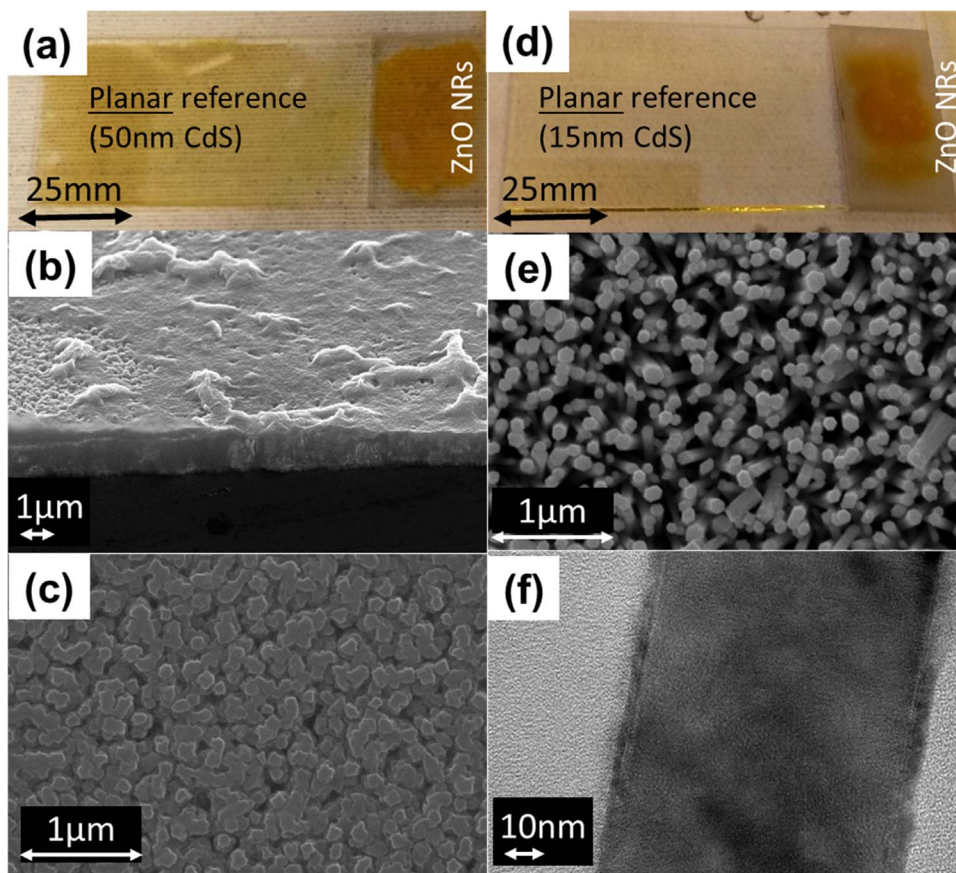
Fig. 2. Effect of CdS deposition time on the structure of CdS/ZnO NRs. (a) A photo of 50 nm film growth (on planar reference). Resulting SEM images showing complete filling of the gaps within the ZnO NR array (b, c). A photo of the planar film with a thickness of 15 nm (d). Resulting SEM and TEM images showing the formation of ZnO/CdS core-shell NRs (e, f). The shell formed on the ZnO core walls, as revealed in (f), is analysed in detail by Fig. 3.
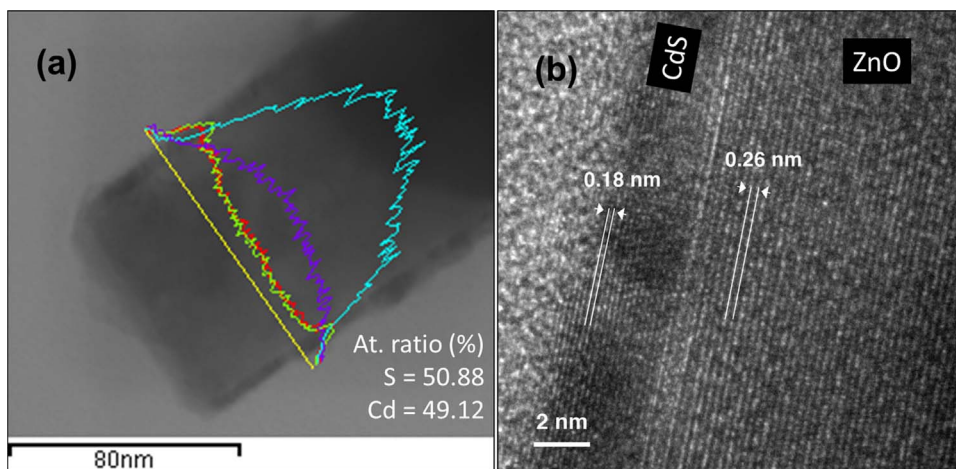

Fig. 3. (a) EDS line profiles collected from a CdS/ZnO core-shell NR: Zn (light blue), O (purple), Cd (green) and S (red). More concentric Cd and S signals at the NR walls indicate the shell to be CdS. (b) A HRTEM image taken at the CdS/ZnO NR interface. (For interpretation of the references to color in this figure legend, the reader is referred to the web version of this article.).

Upon CdTe growth, the width of the individual NRs increased up to 200 nm and some agglomerated NR clusters was also observable where the rod-to-rod separation was very small. The rise in Cd^{114}, Te^{120}, and As^{75} signals with respect to those of Zn^{64} and O^{18} near the base of the NR array is probably due to a change in the density of the ZnO NRs, resulting in a thicker CdTe layer forming at the base region. In the absence of a suitable reference/calibration sample, direct quantification of the As atomic concentration within the CdTe layer was not possible; however, a similarly prepared planar CdTe:As thin film provided a steady As concentration of $\sim 10^{19}$ atoms/cm^3 (not shown here). Notably, As doping at $\sim 10^{18}$ atoms/cm^3 level was found essential for MOCVD thin film devices [22], with thinner absorbers cells requiring even higher dopant concentrations [23].

3.4. Device optical modelling

Fig. 6a and b show the spectrum of light absorbed in each layer for both NR-based and planar surfaces, respectively. At first glance, it can be seen that ITO and ZnO absorb in UV region of the spectrum, especially for wavelengths below 400 nm. The amount of light absorption in ITO (~ 0.65 mA/cm^2) is similar for both cases whereas light absorption in ZnO is higher for NRs. Additionally, ITO weakly absorbs at longer wavelengths, too, due to free carriers.

The absorption in CdS dominates between 350 and 500 nm. The total CdS absorption in NR-based structures is much higher than the planar cells. The AM 1.5 solar spectrum weighed CdS absorption in NR-based cells is 2.33 mA/cm^2 (shown in Fig. 6a) while it is only 0.94 mA/cm^2 (shown in Fig. 6b) for the planar cells. The enhanced parasitic
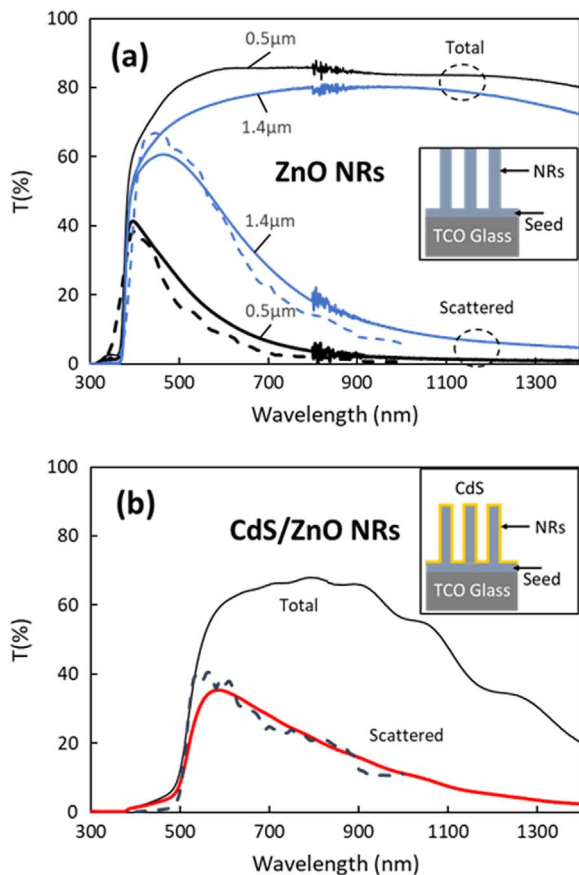
Fig. 4. Total transmittance and scattered light due to ZnO NRs (a) and ZnO/CdS core-shell NRs (with ~ 20 nm CdS shell) (b). Dashed lines are the model results for the corresponding haze data. Insets show schematics of the measured and simulated structures. Note the calculations were made up to 1000 nm, beyond which reliable optical constants could not be found in the literature.

absorption in CdS is due to the increase in the amount of CdS material as it covers the relatively large ZnO NRs' surface area as well as the light trapping effects within the ZnO NR array. For the planar cell, the amount of CdS is not significant to absorb most of the light in the blue region of the spectrum. However, in case of NRs, light scattered by ZnO NRs encounters with the CdS layer first and therefore an increased absorption is unavoidable. To do away with this parasitic absorption an alternative n-type window layer material having higher transparency, such as $Zn_{1-x}Mg_xO$, can be utilized (see Fig. S1 in Supplementary).

For longer wavelengths (500–750 nm), CdTe absorbs almost all the light. The NR-based cells have higher absorption in CdTe at long

wavelengths (> 750 nm) compared to the planar structure due to light trapping effect of NRs. However, the superior absorbance capability of the NR-based structure at long wavelengths is just enough to compensate the enhanced parasitic absorption loss at short wavelengths due to CdS shells. The solar spectrum weighed absorption in CdTe was calculated from 300 to 850 nm to be 24.67 mA/cm^2 for NR-based cells and 24.64 mA/cm^2 for planar cells.

The solar spectrum weighed absorption profile between 300 and 900 nm for the NR and planar structures are shown in Fig. 6c and d, respectively. The red colour represents high absorption and the blue colour represents low absorption while it should be noted that a logarithmic scale normalized to 1 is given. The disorderly formed interference patterns at different angles in NR-based structure confirm its light trapping effects. In NR-based structure, while most of the absorption occurs in CdTe, thin CdS layer also absorbs significantly as indicated by a reddish-yellowish colour. It is also noticeable that CdS absorption is less significant in the planar case. While ITO absorbs moderately, the absorption in ZnO is quite limited in both structures.

3.5. Device performance

In the development of prototype NR-based devices (Fig. 7a), it was considered necessary to avoid all potential electrical shorts between the front contact, i.e. ZnO NR cores, and the back contact (Au), which may arise due to the NR substrate-bound roughness of the grown surfaces. Therefore, adopting the method followed by Fan et al. [9], all the available gaps within the ZnO/CdS core-shell NR arrays was filled with CdTe, also forming a continuous thin film of CdTe atop the NRs, similarly to the simulated "buried" structure. Cross-sectional EDS maps of major elements (Fig. 7c and d) confirm that the ZnO NRs are entirely buried in the CdTe material and hence well separated from the Au contact film. Due to the above mentioned non-uniform growth of CdS on ZnO NRs, the thickness of CdS showed considerable variation as exemplified by EDS images in Fig. 7c and d (cells B4 and C2, respectively). The corresponding light *J-V* curves for these cells indicate the importance of having a CdS window layer between CdTe and ZnO: cell B4 with a CdS window clearly exhibiting better diode characteristics. Furthermore, it was observed that such regions always exhibited better device performance with higher shunt resistance and fill factors compared to cells having CdS deficiency.

The device performance of the best nanostructured solar cell is compared to that of a planar thin film structure deposited in the same (MOCVD) growth run (Fig. 8). As previously noted, the CdS thickness and growth rate was much higher on the ZnO NRs, than for the planar device. Thus the resulting nanostructured solar cells showed a lower J_{sc} (by ~ 5 mA cm^{-2}), but surprisingly, an improved *FF* (by ~ 10%) and V_{oc} (by 20 mV) was obtained. Device efficiencies were comparable; however, several shunted cells were also observed for the planar device probably resulting from poor coverage of the CdS window. The better
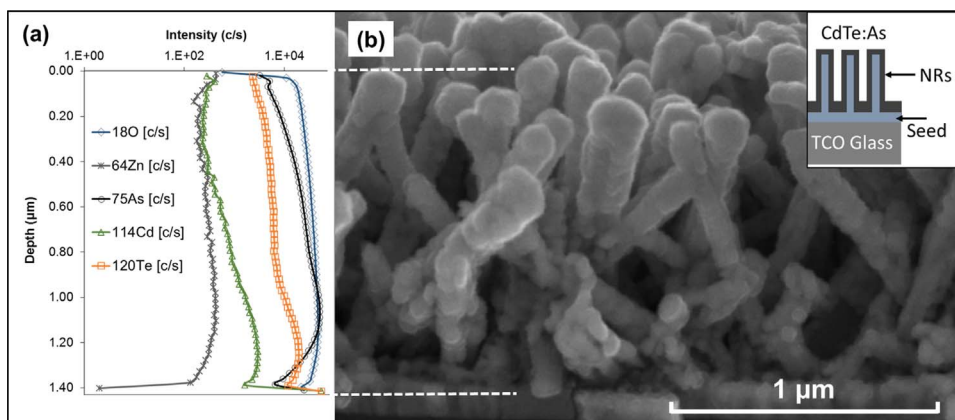

Fig. 5. SIMS depth profiles of the Zn^{64}, O^{18}, Cd^{114}, Te^{120}, and As^{75} isotopes (a) and a cross-sectional SEM image (b) for a CdTe:As coated ZnO NR array with rod length of ~ 1.4 μm.
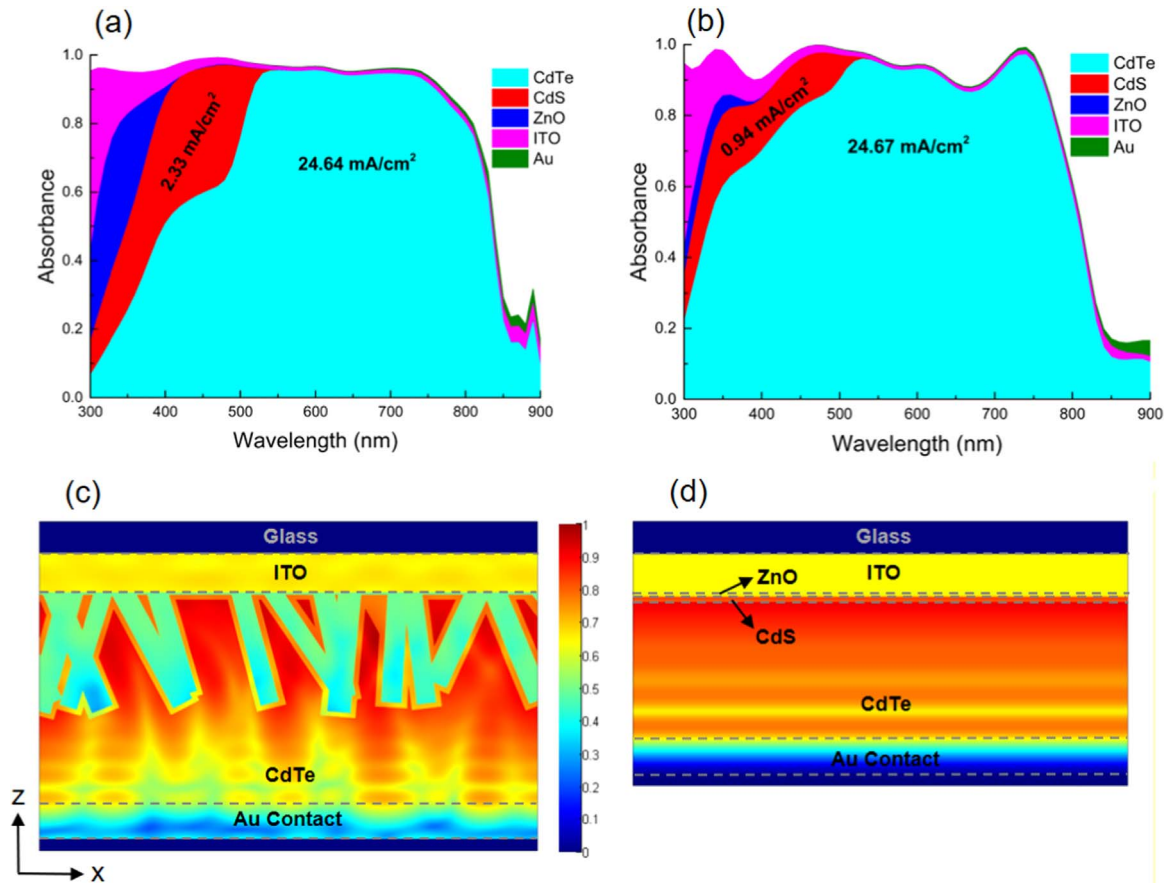
Fig. 6. The absorption spectra in each layer for (a) NR-based and (b) planar cells. The corresponding solar spectrum weighed normalized absorption profiles are given for (c) NR-based cells and (d) planar cells.

FF for the NR-based solar cells is particularly encouraging as it indicates good coverage of the window layer on the rough ZnO NR arrays by the MOCVD method. However, the deposition uniformity needs to be improved using a suitable surface preparation method such as mild plasma treatment [24]. Achieving high spatial uniformity with the CdTe/CdS/ZnO NR structure would enable the development of larger area devices.

The EQE response of the planar devices showed a better collection both in the blue/near UV (due to low absorption by the ultrathin CdS) and in the red region between 650–830 nm. In agreement with the simulations (see Fig. 6d) the blue part of the spectrum is strongly absorbed by CdS layer and causes J_{sc} losses in the case of ZnO NR array. Volume thickness of the absorber deposited on the NRs and planar
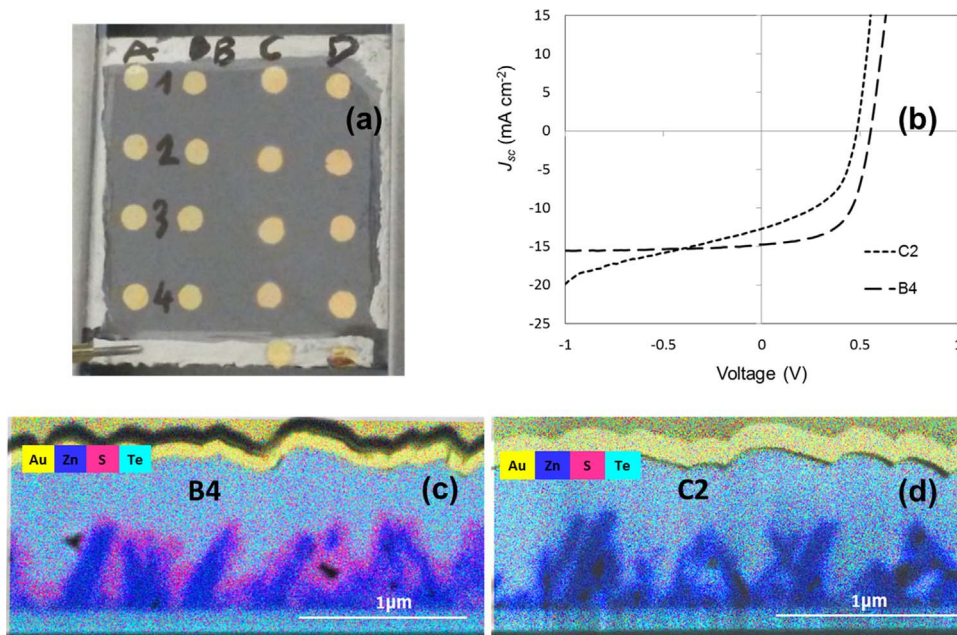

Fig. 7. A typical 2.5 × 2.5 cm^2 CdTe/CdS/ZnO NRs device with 2 mm diameter dot contacts (a), light *J-V* curves (b) and cross-sectional EDS elemental (Au, Zn, S, and Te) maps (c, d) for selected cells (B4, C2). ZnO NRs in cell B4 have a CdS coating whereas those in C2 has little/or no CdS coverage. The ZnO NRs are embedded in a relatively thick CdTe layer electrically separating the Au contact.
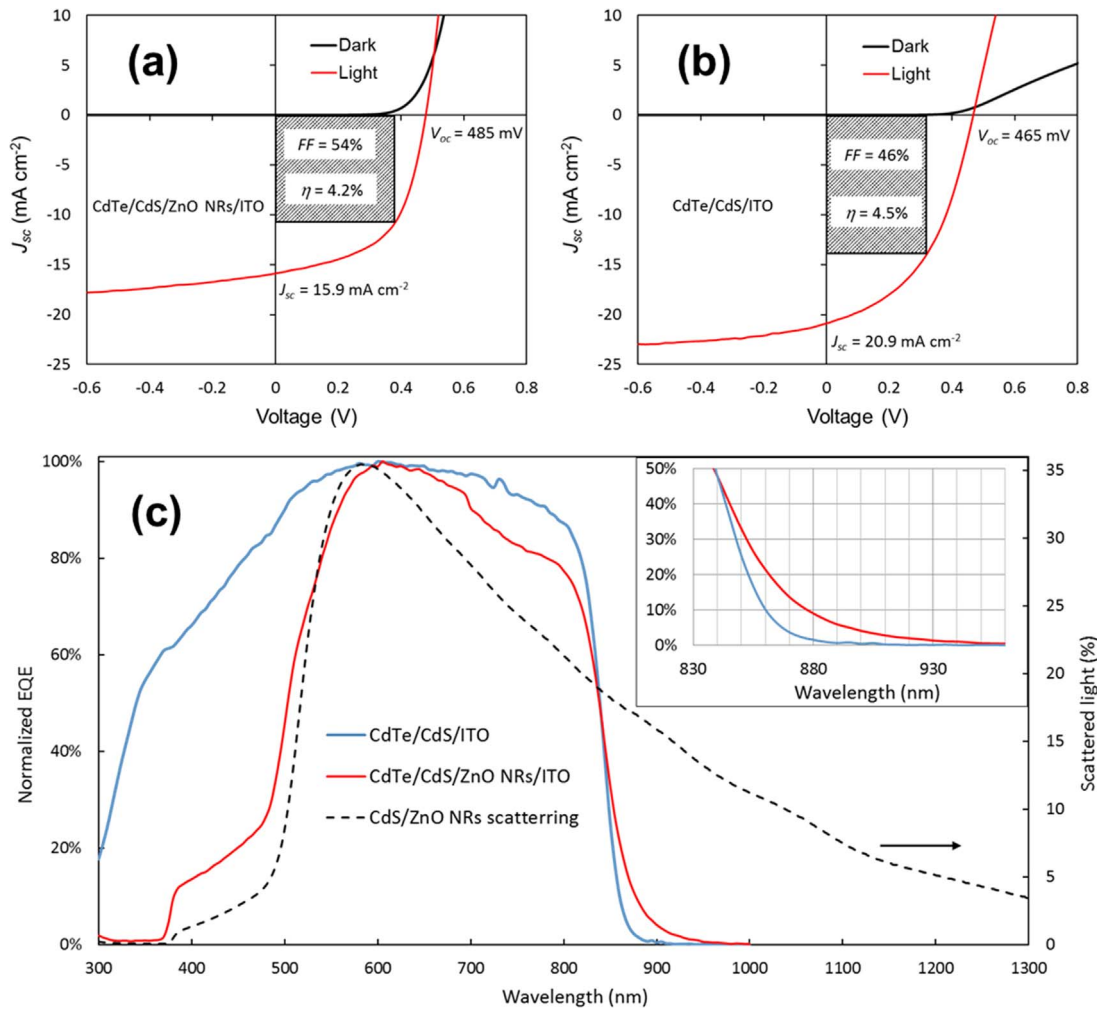
Fig. 8. IV curves (a, b) and EQE spectra (c) of the best CdTe/CdS/ZnO NRs/ITO and planar CdTe/CdS/ITO solar cells. The scattered component of the transmitted light from a CdS/ZnO core-shell NRs array is also shown in (c) for comparison. The improved collection for the CdTe/CdS/ZnO NRs/ITO device in the near IR is highlighted in the inset to (c).

substrate was determined to be about 400 and 550 nm, respectively. This supports the observation of poorer red response with the NR-device. On the other hand, the NR-based cells show an improved collection in the near IR, around 900 nm (see inset to Fig. 8c). When compared to the light scattering from a CdS/ZnO NR array (dashed line, Fig. 8c) it can be understood that this gain is due to light trapping, a prominent feature of the one-dimensional nanostructures such as the NRs.

4. Discussion

Data in Fig. 7 showed that the NR device with a CdS window layer exhibits improved diode characteristics, due to higher shunt resistance and fill factors, when compared to cells having CdS deficiency. In relation to this observation, it is noteworthy to mention the study of Zhang et al. [7]. They attested the contribution of an ultrathin (0–8 nm) CdS film (inner shell) between the CdTe absorber (outer shell) and ZnO nanorods (core), where CdS and CdTe were deposited by the SILAR method, showing that cell efficiency increased from ~ 0.2% for no CdS (0 nm) case to ~ 0.7% for 4–8 nm CdS with ~ 200 nm thick CdTe absorber (see also Table 1). The improvement was attributed to passivation of the ZnO NRs' surface using CdS (deduced from photoluminescence spectra) as well as the graded band energy alignment, expected of the ZnO/CdS/CdTe structure.

Due to the lack of suitable planar cell structure (with equal amounts of semiconductor layers as the NR cells), it was not possible to clearly

demonstrate the advantages and disadvantages of having a core-shell NR cell structure. Rekemayer et al. fabricated PbS based solar cells on ZnO NRs via a layer-by-layer chemical deposition method and measured a net J_{sc} gain (of ~ 4 mA cm^{-2}) compared to equivalently grown planar solar cell [25]. Overall, device conversion efficiency was also improved by 0.5–1% (absolute) for the nanostructured cells. Their reflectance and internal quantum efficiency data lead to the conclusion that both light trapping (leading to enhanced absorption) and carrier collection efficiency (due to the shorter path required for carriers to cross) with the core-shell NR geometry were responsible for the enhancements. Further, it is remarkable that they also noticed a gain in photo-response near the absorption edge of the absorber (~ 1000 nm for PbS) which was assigned to the light trapping effect. This effect was suggested to increase the optical path length in the absorber and thereby enable capturing of the weakly absorbed near IR photons.

A recent report by Major et al., who fabricated a CdTe solar cell structure on ZnO NR array films, appears relevant to this study [26]. In their approach, the ZnO NR film is believed to have served as a highly resistive buffer layer, as it was found that a core-shell structure was not achieved via the deposition method used. Therefore, it is not possible to make a direct comparison with our study in regards to core-shell nanorod geometry and light trapping.

On a further note, performance of NR vs. planar CdTe devices, employing equal amount of absorber, was studied via electrical modelling. We compared planar and NR-based CdTe solar cells in terms of various CdTe base doping densities (1×10^{15}, 1×10^{16} and $1 \times$
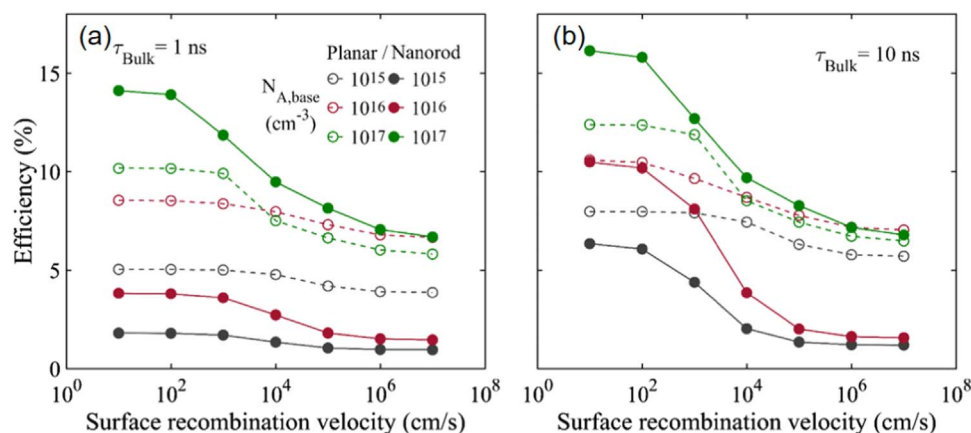
10^{17} cm^{-3}), minority carrier lifetimes (1 and 10 ns) and surface recombination velocities (between 1×10^{1} and 1×10^{7} cm/s).

NR-based CdTe solar cells suffer significantly from carrier recombinations due to enhanced CdTe/CdS interface area as shown in Fig. 9a and b. Therefore, their efficiencies drop significantly with surface recombination velocity at the interface. In the literature, there are reports with achieved surface recombination velocities below 100 cm/s at the CdTe/CdS interface [27]. Thus, it should be noted that 1×10^{7} cm/s represents a very poor surface passivation. 1–10 ns minority carrier lifetime (τ_{Bulk}) and $1 \times 10^{15} - 1 \times 10^{17}$ cm^{-3} doping concentration covers the state-of-the-art as well as the projected values in the literature [28].

Fig. 9a and b show that even when very good surface passivation and bulk material quality are achieved high doping densities are necessary for the NR-based solar cell to outperform its planar counterpart. When a 1 ns bulk lifetime is assumed (Fig. 9a), NR-based devices with 1×10^{15} and 1×10^{16} cm^{-3} base doping densities perform much inferior to the planar ones. Even though this efficiency gap can be lowered with increasing bulk quality (τ_{Bulk} = 10 ns, Fig. 9b), doping densities above 1×10^{16} cm^{-3} are still required to promote NR-based CdTe solar cells.

5. Conclusions

ZnO NR arrays were utilized to study the deposition behaviour, optical and photovoltaic response of the CdS/CdTe semiconductor films by MOCVD. Optical simulations indicated that light trapping effect of ZnO NRs yields an enhancement in J_{sc} at wavelengths longer than 700 nm while it also causes an increased parasitic loss due to light absorption in CdS for wavelengths between 350 and 500 nm. The much shortened nucleation delay and higher growth rate for CdS deposition on ZnO NRs played an important role in determining the overall core-shell NRs structure and their properties compared to planar counterpart samples. Solar cells prepared via As doping of the CdTe absorber showed similar conversion efficiencies for both nanostructured (CdTe/CdS/ZnO NRs/ITO) and planar (CdTe/CdS/ITO) solar cells, given the experimental variations in the thickness and absorption characteristics of CdS and CdTe layers in these configurations. Deposition uniformity will need to be increased to allow more systematic studies towards increasing performance of such nanostructured devices. The light trapping, emanating from the scattering due to underlying ZnO/CdS NR array structure, was observed to contribute to the better spectral response of the nanostructured solar cells in the near IR range (830–930 nm). Electrical simulations indicate that NR-based solar cells can outperform their planar counterparts having the same amount of active material provided high doping concentrations and low CdTe/CdS surface recombination velocities are achieved. Overall, these results show that the CdTe/CdS/ZnO NRs/ITO solar cell structure with

engineered optical properties has good potential for the improvement of extremely-thin-absorber (eta) CdTe solar cells.

Appendix A. Supplementary material

Supplementary data associated with this article can be found in the online version at http://dx.doi.org/10.1016/j.solmat.2017.11.036.

References

[1] M.A. Green, K. Emery, Y. Hishikawa, W. Warta, E.D. Dunlop, Solar cell efficiency tables (version 48), Prog. Photovolt.: Res. Appl. 24 (2016) 905–913.

[2] V. Plotnikov, X. Liu, N. Paudel, D. Kwon, K.A. Wieland, A.D. Compaan, Thin-film CdTe cells: reducing the CdTe, Thin Solid Films 519 (2011) 7134–7137.

[3] M.D. Kelzenberg, S.W. Boettcher, J.A. Petykiewicz, D.B. Turner-Evans, M.C. Putnam, E.L. Warren, J.M. Spurgeon, R.M. Briggs, N.S. Lewis, H.A. Atwater, Enhanced absorption and carrier collection in Si wire arrays for photovoltaic applications, Nat. Mater. 9 (2010) 239–244.

[4] B. Luo, Y. Deng, Y. Wang, M. Tan, L. Cao, Independent growth of CdTe nanorod arrays on different substrates with enhanced photoelectrical property, J. Nanopart. Res. 14 (946) (2012) 1–8.

[5] V. Consonni, S. Renet, J. Garnier, P. Gergaud, L. Artús, J. Michallon, L. Rapenne, E. Appert, A. Kaminski-Cachopo, Improvement of the physical properties of ZnO/CdTe core-shell nanowire arrays by CdCl$_2$ heat treatment for solar cells, Nanoscale Res. Lett. 9 (222) (2014) 1–13.

[6] X. Wang, H. Zhu, Y. Xu, H. Wang, Y. Tao, S. Hark, X. Xiao, Q. Li, Aligned ZnO/CdTe core-shell nanocable arrays on indium tin oxide: synthesis and photoelectrochemical properties, ACS Nano 4 (2010) 3302–3308.

[7] G. Zhang, S. Jiang, Y. Lin, W. Ren, H. Cai, Y. Wu, Q. Zhang, N. Pan, Y. Luo, X. Wang, Improving the photovoltaic performance of solid-state ZnO/CdTe core–shell nanorod array solar cells using a thin CdS interfacial layer, J. Mater. Chem. A 2 (2014) 5675–5681.

[8] B.L. Williams, A.A. Taylor, B.G. Mendis, L. Phillips, L. Bowen, J.D. Major, K. Durose, Core-shell ITO/ZnO/CdS/CdTe nanowire solar cells, Appl. Phys. Lett. 104 (053907) (2014) 1–5.

[9] Z. Fan, H. Razavi, J.W. Do, A. Moriwaki, O. Ergen, Y.L. Chueh, P.W. Leu, J.C. Ho, T. Takahashi, L.A. Reichertz, S. Neale, K. Yu, M. Wu, J.W. Ager, A. Javey, Three-dimensional nanopillar-array photovoltaics on low-cost and flexible substrates, Nat. Mater. 8 (2009) 648–653.

[10] M.C. Akgun, Y.E. Kalay, H.E. Unalan, Hydrothermal zinc oxide nanowire growth using zinc acetate dihydrate salt, J. Mater. Res. 27 (2012) 1445–1451.

[11] G. Kartopu, A.J. Clayton, W.S.M. Brooks, S.D. Hodgson, V. Barrioz, A. Maertens, D.A. Lamb, S.J.C. Irvine, Effect of window layer composition in Cd$_{1-x}$Zn$_x$S/CdTe solar cells, Prog. Photovolt.: Res. Appl. 22 (2014) 18–23.

[12] G. Kartopu, L.J. Phillips, V. Barrioz, S.J.C. Irvine, S.D. Hodgson, E. Tejedor, D. Dupin, A.J. Clayton, S.L. Rugen-Hankey, K. Durose, Progression of metalorganic chemical vapour-deposited CdTe thin-film PV devices towards modules, Prog. Photovolt.: Res. Appl. 24 (2016) 283–291.

[13] T.A.F. König, P.A. Ledin, J. Kerszulis, M.A. Mahmoud, M.A. El-Sayed, J.R. Reynolds, V.V. Tsukruk, Electrically tunable plasmonic behaviour of nanocube-polymer nanomaterials induced by redox-active electrochromic polymer, ACS Nano 8 (2014)

6182–6192.

[14] Z. Holman, et al, unpublished data, retrieved from ⟨https://www2.pvlighthouse.com.au⟩ on 17/11/2017.

[15] R.E. Treharne, A. Seymour-Pierce, K. Durose, K. Hutchings, S. Roncallo, D. Lane, Optical design and fabrication of fully sputtered CdTe/CdS solar cells, J. Phys. Conf. Ser. 286 (2011) 1–8.

[16] K.M. McPeak, S.R. Jayanti, S.J.P. Kress, S. Meyer, S. Iotti, A. Rossinelli, D.J. Norris, Plasmonic films can easily be better: rules and recipes, ACS Photonics 2 (2015) 326–333.

[17] M. Burgelman, P. Nollet, S. Degrave, Electrical behaviour of thin-film CdTe solar cells, Appl. Phys. A 69 (1999) 149–153.

[18] M. Gloeckler, A.L. Fahrenbruch, J.R. Sites, Numerical modeling of CIGS and CdTe solar cells: setting the baseline, In: Proceedings of the 3rd World Conference on Photovoltaic Energy Conversion, 2003, pp. 491–494.

[19] M. Burgelman, P. Nollet, S. Degrave, Modelling polycrystalline semiconductor solar cells, Thin Solid Films 361–362 (2000) 527–532.

[20] T. Minami, T. Miyata, T. Yamamoto, Work function of transparent conducting multicomponent oxide thin films prepared by magnetron sputtering, Surf. Coat. Technol. 108–109 (1998) 583–587.

[21] B. Höffling, A. Schleife, F. Fuchs, C. Rödl, F. Bechstedt, Band lineup between silicon and transparent conducting oxides, Appl. Phys. Lett. 97 (2010) 1–3.

[22] S.J.C. Irvine, V. Barrioz, D. Lamb, E.W. Jones, R.L. Rowlands-Jones, MOCVD of thin film photovoltaic solar cells—next generation production technology? J. Cryst.

Growth 310 (2008) 5198–5203.

[23] A.J. Clayton, S.J.C. Irvine, E.W. Jones, G. Kartopu, V. Barrioz, W.S.M. Brooks, MOCVD of $Cd_{(1-x)}Zn_{(x)}S$/CdTe PV cells using an ultra-thin absorber layer, Sol. Energy Mater. Sol. Cells 101 (2012) 68–72.

[24] D.E. Swanson, R.M. Geisthardt, J.T. McGoffin, J.D. Williams, J.R. Sites, Improved CdTe solar-cell performance by plasma cleaning the TCO layer, IEEE J. Photovolt. 3 (2013) 838–842.

[25] P. Rekemeyer, S. Chang, C.H.M. Chuang, G.W. Hwang, M.G. Bawendi, S. Gradečak, Enhanced photocurrent in PbS quantum dot photovoltaics via ZnO nanowires and band alignment engineering, Adv. Energy Mater. 6 (1600848) (2016) 1–7.

[26] J.D. Major, R. Tena-Zaera, E. Azaceta, L. Bowen, K. Durose, Development of ZnO nanowire based CdTe thin film solar cells, Sol. Energy Mater. Sol. Cells 160 (2017) 107–115.

[27] J.M. Burst, J.N. Duenov, D.S. Albin, E. Colegrove, M.O. Reese, J.A. Aguiar, C.S. Jiang, M.K. Patel, M.M. Al-Jassim, D. Kuciauskas, S. Swain, T. Ablekim, K.G. Lynn, W.K. Metzger, CdTe solar cells with open-circuit voltage breaking the 1 V barrier, Nat. Energy 1 (2016) 1–7.

[28] J.M. Burst, J.N. Duenov, A. Kanevce, H.R. Moutinho, C.S. Jiang, M.M. Al-Jassim, M.O. Reese, D.S. Albin, J.A. Aguiar, E. Colegrove, T. Ablekim, S.K. Swain, K.G. Lynn, D. Kuciauskas, T.M. Barnes, W.K. Metzger, Interface characterization of single-crystal CdTe solar cells with $V_{OC} > 950$ mV, IEEE J. Photovolt. 6 (2016) 1650–1653.